JACS
JOURNAL OF THE AMERICAN CHEMICAL SOCIETY

Article

pubs.acs.org/JACS

Directly Probing the Effects of Ions on Hydration Forces at Interfaces

Jason I. Kilpatrick,*[,‡] Siu-Hong Loh,[†,‡] and Suzanne P. Jarvis

Conway Institute of Biomolecular and Biomedical Research, University College Dublin, Belfield, Dublin 4, Ireland

Supporting Information

ABSTRACT: Understanding the influence of water layers adjacent to interfaces is fundamental in order to fully comprehend the interactions of both biological and nonbiological materials in aqueous environments. In this study, we have investigated hydration forces at the mica−electrolyte interface as a function of ion valency and concentration using subnanometer oscillation amplitude frequency modulation atomic force microscopy (FM-AFM). Our results reveal new insights into the nature of hydration forces at interfaces due to our ability to measure high force gradients without instability and in the absence of lateral confinement due to the use of an atomically sharp tip. We demonstrate the influence of electrolytes on the properties of both primary and structural hydration forces and reveal new insights into the interplay between these phenomena in determining the interaction forces experienced by a nanoscale object approaching an interface. We also highlight the difficulty in directly comparing hydration force data from different measurement techniques where the nature of the perturbation induced by differing interaction geometries is likely to dramatically affect the results.

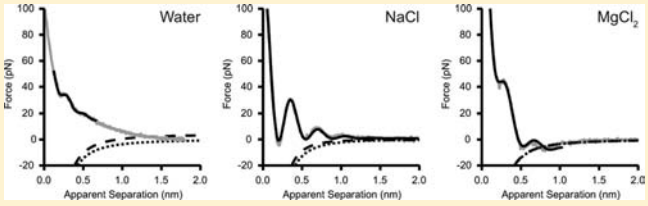

INTRODUCTION

The role of hydration forces at interfaces is fundamental to our understanding of the interactions of both biological and nonbiological materials in aqueous environments. Previous studies have revealed the presence of short-range repulsive interactions attributed to hydration forces at a variety of interfaces including mica,[1] silica,[2] lipid bilayers,[3] surfactants,[4] DNA,[5] and proteins.[6] Such ubiquity clearly demonstrates the importance of these forces in determining aqueous interactions, but such forces cannot be explained by classic continuum models such as the Derjaguin−Landau−Verwey−Overbeek (DLVO) theory of colloid stability. DLVO theory, which is a summation of the repulsive electrolytic entropic force with the attractive van der Waals force, provides a good approximation for the interaction of surfaces at separations exceeding a few nanometers and at low salt concentrations (<10 mM)[7] but fails to predict forces at smaller separations where the discrete nature of the solvent, electrolyte, and the surface itself become significant.[8] Large repulsive forces observed at these small separations are typically ascribed to hydration forces, the origin of which remains unclear and continues to be a topic of great interest.[7,9] A wide range of factors contributing to hydration forces have previously been proposed, including solvent volume exclusion, specific ion effects, polarizability, ionic dispersion interactions, and modification of the dielectric properties of water at the interface. Previous reports have classified hydration forces into three categories, each with a characteristic decay length (λ): primary hydration forces, due to the removal of water molecules bound directly to the interface (λ = 2−4 Å);[9] secondary hydration forces, due to the interaction of hydrated ions (λ = 10−30 Å);[7] and structural hydration forces, resulting from steric effects due to the finite volume of the solvent molecules resulting in an oscillatory force profile (λ = 1−3 Å).[10] The charge and polarizability of the interface and surrounding ions, ion valency, and concentration are all expected to play a role in determining the relative magnitude of each type of hydration force observed.[8] Additional mechanisms may also be present at high salt concentrations and confined geometries, including ion exclusion from the surface hydration layer (consistent with primary hydration forces) and ionic dispersion forces that modify the entropic force contribution by altering ion distribution at the interface (consistent with secondary hydration forces), both of which result in additional repulsive forces.[7,11] For the purposes of this study, the term primary hydration force is used to describe a monotonically decaying force with a short decay length (λ = 2−4 Å). We do not attempt to distinguish between different mechanisms that may give rise to this force as it is still a topic of debate in the literature.[7,9] Instead, we use this term in a descriptive manner to discuss the observed behavior rather than attempting to assign its origin. Here we build upon previous measurements with the surface forces apparatus (SFA)[1,2,12−16] and the atomic force microscope (AFM)[10,17−21] and on theoretical studies[22−27] of hydration forces adjacent to an interface in electrolyte solutions. By employing subnanometer oscillation amplitude frequency modulation (FM) AFM combined with a bespoke low-noise AFM and atomically sharp tips, we are able to investigate the nature of hydration forces in the presence of electrolytes as a function of ion valency and concentration without inducing lateral confinement, which occurs with blunt AFM tips and SFA measurements.[28] This technique, whereby a very stiff cantilever can be used without sacrificing sensitivity, enables us to directly

Received: October 17, 2012
Published: February 11, 2013

measure high force gradients with piconewton force sensitivity without suffering from cantilever instabilities or hysteresis.[10,28]

MATERIALS AND METHODS

Sample Preparation. Two single-component electrolyte solutions (NaCl and $MgCl_2$) were prepared by dissolving high purity grade salts (Sigma–Aldrich, Dublin, Ireland) as received in pure water (Milli-Q water, 18.3 MΩ·cm). High-grade V-1 muscovite mica discs (SPI supplies, West Chester, PA) were glued onto a Teflon substrate and then cleaved with adhesive tape immediately prior to liquid deposition. Solution (100 μL) was then deposited onto the freshly cleaved mica surface and the substrate holder was placed in the AFM for measurements after a suitable period of equilibration.

Atomic Force Microscope Measurements. A bespoke low-noise AFM[29] combined with an Asylum Research bipolar controller (Santa Barbara, CA) operating in FM mode was used for all measurements. In FM mode the cantilever oscillation amplitude was maintained at a constant value (~2.5 Å) by one feedback loop, while a second feedback loop tracked changes in the resonant frequency due to tip–sample interactions. Automated gain calculation algorithms were employed to ensure robust feedback loop tuning.[30] Force versus distance curves were obtained as frequency shift versus distance while operating at the fundamental resonance frequency of the cantilever. Force versus distance curves were then calculated by the method of Sader and Jarvis.[31] Gold-coated (detector side) silicon cantilevers with tip radius <2 nm (Nanosensors: SSS-NCHAuD) and a nominal spring constant of 10–20 N/m were used for all measurements. The spring constant was determined for each cantilever prior to measurements by the method of Hutter and Bechhoefer.[32] Force curves presented in this study show approach curves only for clarity, with retract curves showing no evidence of hysteresis. Some thermal drift effects were evident (average drift rate <50 pm/s).

RESULTS AND DISCUSSION

Force versus distance curves were acquired for the interaction between an atomically sharp tip and a freshly cleaved mica surface in 150 mM NaCl at an approach rate of 1 nm/s. The resulting frequency shift versus distance curve (Figure 1a) shows a decaying oscillatory profile indicative of structural hydration forces with two peaks clearly visible. For values below the maxima of the primary hydration peak, multiple tip–sample distances have equivalent frequency shifts as indicated by points i and ii, which occur at a separation of ~2.3 Å (comparable with the size of a single water molecule). When surfaces are imaged at the atomic scale in electrolyte solutions, this energy barrier results in a quasi-stable condition enabling imaging to be performed directly upon the primary hydration shell (ii) adjacent to the interface[10] (see Supporting Information). Quantification of the tip–sample force is then achieved by conversion of the measured frequency shift to force versus distance by the method of Sader and Jarvis[31] (Figure 1b).

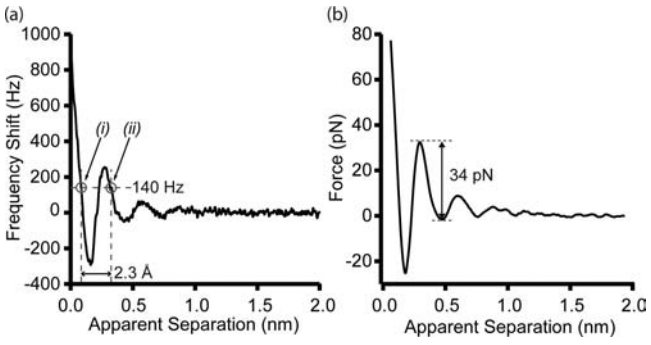

Figure 1. (a) Frequency shift vs distance between an atomically sharp tip and freshly cleaved mica surface in 150 mM NaCl, showing a decaying oscillatory force profile indicative of structural hydration forces (data smoothed by a factor of 10). Tip approach velocity was 1 nm/s, resonant frequency in liquid was ~95 kHz, and spring constant was ~24 N/m. Points i and ii show the location of an equivalent frequency shift (140 Hz) with a spacing of ~2.3 Å. (b) Force vs distance calculated from panel a (data smoothed by a factor of 20). The vertical arrow indicates the magnitude of the primary hydration peak adjacent to the surface (F_{pk} = 34 pN).

Previous studies have demonstrated that ion concentration plays an important role in determining the nature and magnitude of hydration forces.[14,33] To examine these effects, force curves were collected in the presence of a symmetric monovalent salt (NaCl) for concentrations in the range 0–500 mM (Figure 2). From Figure 2 it is clear that at small separations the interaction between the tip and sample is dominated by nonlinear forces that increase in magnitude with decreasing separation. We ascribe the observed behavior to hydration forces comprising a combination of both structural and primary hydration repulsion.[16]

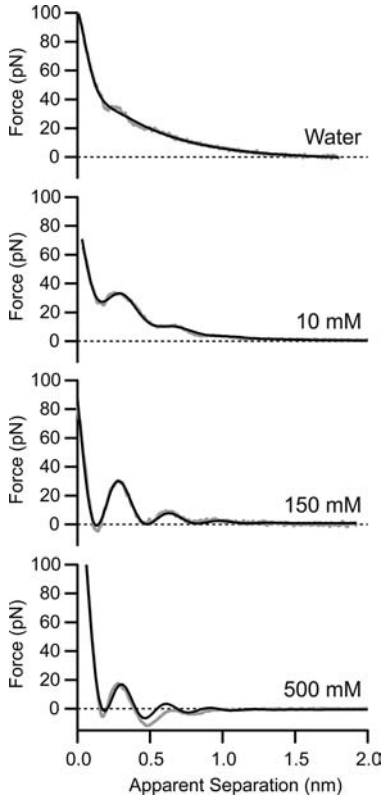

Figure 2. Average force versus distance curves taken in water (n = 30), 10 mM NaCl (n = 13), 150 mM NaCl (n = 30), and 500 mM NaCl (n = 30). Tip approach velocity was 1 nm/s, resonant frequency in liquid was 90–110 kHz, and spring constant was 10–25 N/m. Two cantilevers were used to collect the data; one for water and 150 mM NaCl and another for 10 and 500 mM NaCl. Data were smoothed by a factor of 2 prior to averaging and then subsequently smoothed by a factor of 10 (2000 data points per curve). Gray, averaged data; black, fit to data with eq 1. Data were offset laterally to align the primary hydration peak at 2.8 Å prior to fitting.

In order to quantify such data, we must first consider the relationship between structural and primary hydration forces. While previous studies employ a method of subtracting the calculated DLVO interaction from the measured force in order

dx.doi.org/10.1021/ja310255s | J. Am. Chem. Soc. 2013, 135, 2628–2634

Table 1. Fitting Parameters for NaCl Solutions

NaCl conc, mM	A_S, mJ·m^{-2}	λ_S, Å	σ_S, Å	A_P, mJ·m^{-2}	λ_P, Å
0[a]	2.1 ± 0.14	0.65 ± 0.02	2.18 ± 0.02	9 ± 0.06	4.85 ± 0.04
10	4.5 ± 0.06	2.33 ± 0.03	3.80 ± 0.01	11 ± 0.04	3.32 ± 0.01
150	8.1 ± 0.05	2.43 ± 0.02	3.47 ± 0.01	8 ± 0.05	2.36 ± 0.02
500	7.6 ± 0.21	2.37 ± 0.06	2.99 ± 0.01	23 ± 0.42	0.93 ± 0.01

[a]Full fit values: A_S = 9.7 ± 0.41 mJ·m^{-2}, λ_S = 1.85 ± 0.09 Å, and σ_S = 4.43 ± 0.07 Å. Structural hydration parameters are from partial fit (shown in Figure 3).

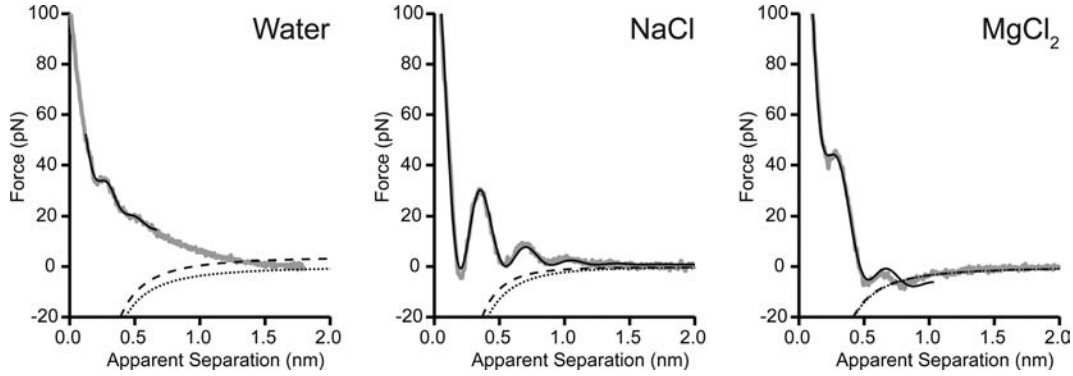

Figure 3. Averaged force versus distance curves (n = 30) measured in pure water, 150 mM NaCl, and 150 mM $MgCl_2$. Tip approach velocity was 1 nm/s, resonant frequency in liquid was ∼95 kHz, and spring constant was ∼24 N/m. All force curves were acquired with the same cantilever. Data were smoothed by a factor of 2 prior to averaging and subsequently smoothed by a factor of 10 (2000 data points per curve). Gray, averaged data; black, fit to data with eq 1. DLVO values were calculated for constant charge (---) and constant potential (···) boundary conditions and scaled by R = 1 nm. Surface potentials: water −150 mV, NaCl −25 mV, and $MgCl_2$ −10 mV. Concentrations: water 0.01 mM, NaCl 150 mM, and $MgCl_2$ 150 mM. Nonretarded Hamaker constant $A_H = 2.2 \times 10^{-20}$ J.

to isolate the hydration forces,[2] we decided not to adopt this methodology since DLVO theory is generally an inadequate descriptor of noncontinuum forces at such small separations and high salt concentrations.[8,34] Additional technical limitations also prohibit a meaningful isolation of non-DLVO forces: the radius of the tip cannot be verified (apart from being able to resolve atomic resolution images), absolute separation cannot be determined, and the measured forces are relative to the value at the maximum separation (due to the nature of the frequency to force conversion).[31] Despite these limitations, we can effectively model the interactions due to hydration forces at small separations as a function of tip−surface separation (D) as a linear combination of structural and primary hydration forces (note that our model does not specifically include secondary hydration forces, ionic dispersion interactions, or contributions from continuum theories such as DLVO):[35]

$$F_{hyd} = 2\pi R\{A_S \cos[2\pi(D + \varphi)/\sigma_S]e^{-D/\lambda_S} + A_P e^{-D/\lambda_P}\} + \delta \quad (1)$$

where A_S and A_P are the magnitudes of structural and primary hydration forces, φ is the phase shift (accounts of unknown zero separation), σ_S is the structural hydration layer spacing, λ_S and λ_P are the decay lengths of structural and primary hydration forces, R is the tip radius, and δ is an offset (accounts for the forces being relative to the value at maximum separation). Note the last term inside the braces accounts for a monotonically decaying repulsive force regardless of its origin.[35,36] We refer to this term as the primary hydration force for the purposes of this study.

By fitting the data to eq 1, we can characterize the parameters of both the structural and primary hydration forces (as shown in Table 1). Since our model does not include attractive force contributions, such as those arising from van der Waals interactions, the quality of fitting for the 500 mM case, where some attraction is observed, was diminished. From Figure 2 we can observe that increasing the concentration of cations resulted in a reduction in the decay length of the primary hydration force, while the structural hydration force spacing and decay length remained constant. The changes in primary hydration force with concentration observed here are similar to those reported previously for silica suspensions.[37]

Previously, studies have shown that, for mica, increasing cation hydration and concentration increases the magnitude and range of the secondary hydration forces above a critical concentration threshold.[12,16] Other studies have reported opposing observations for silica surfaces with no concentration effects observed.[2,38] In our study, which combines an atomically sharp silicon tip with a planar mica surface, we observe an intermediate case where the magnitude of the primary hydration force increases with concentration but the decay length decreases (Table 1). We see no evidence of secondary hydration forces in our measurements with all decay lengths observed below 5 Å. Importantly, we observe that the magnitude of the structural hydration force is directly influenced by the properties of the primary hydration force. Here we observe an increase in A_S with increasing cation concentration, where a corresponding reduction in the decay length of the primary hydration is observed. The nonadditive behavior of these two forces suggests that they are detected via different mechanisms.

Increasing cation concentration results in a reduction of the short-range repulsive hydration forces with respect to the attraction due to van der Waals interactions. For the condition where these two forces are of similar magnitude, we observe a maximum in the structural hydration force (∼150 mM NaCl).

Controlling the influence of the primary hydration force by adjusting the cation concentration can therefore be utilized as a means to either enhance or mask the presence of the structural hydration forces adjacent to an interface. This leads to a mechanism whereby cation concentration can be utilized to optimize lateral resolution by adjusting the force gradient adjacent to an interface (demonstrated by true atomic resolution in aqueous environments) and to control the probability of stable imaging occurring upon a hydration energy barrier (see Supporting Information).

To investigate the interplay between ion concentration and ion valency (density and distribution of charge at the interface), the influence of cation valency on hydration forces was investigated for three systems: pure water, monovalent cation (150 mM NaCl), and divalent cation (150 mM $MgCl_2$) solutions at the mica interface (Figure 3). Note that for the data presented in Figure 3, the same AFM cantilever was used for all measurements in the sequence NaCl, $MgCl_2$, and pure water. These measurements were subsequently verified by use of a different cantilever in the sequence $MgCl_2$, NaCl, and pure water (data not shown). By using the same cantilever for all measurements, a self-consistent comparison can be made with experimental uncertainties such as tip radius being minimized. As mentioned above, it is unlikely that DLVO theory will be an adequate descriptor for interactions at these length scales and ion concentrations, but we include the results of such calculations for completeness and to aid in comparison to other studies. Thus, the electrolytic entropic repulsion F_{EL} was calculated for a parabolic tip interacting with a flat surface in the low-potential limit for constant charge and constant potential boundary conditions.[35] These boundary conditions represent the upper and lower bounds of the electrostatic double-layer entropic repulsion for the continuum model, and the derivation of these expressions can be found elsewhere.[39,40] Data were recorded in a 2 nm region adjacent to the interface in this study in order to maximize the data available in the region where hydration forces occur. As such, there was insufficient data at larger separations to fit parameters such as surface potential and Debye length, as is common practice. Consequently, calculations were based upon literature values for surface potential,[2,14,41] and Debye lengths were calculated from the solution concentration and valency of the cations. The attraction due to the van der Waals interactions were calculated as $F_{vdW} = -A_H R/6D^2$, where D is the distance between the tip and sample, and we use a nonretarded Hamaker constant $A_H = 2.2 \times 10^{-20}$ J. The total interaction force according to the continuum DLVO theory is then the summation of these forces: $F_{DLVO} = F_{EL} + F_{vdW}$.

Over 200 force curves were obtained for each solution, which were classified according to the number of structural hydration layers observed (Table 2). No more than three hydration layers were observed, with one layer most frequently observed for water (~65%) and two layers most frequently observed for NaCl (~67%) and $MgCl_2$ (~64%) solutions. Data from Figure 3 were fitted with eq 1 in order to obtain information about the influence of valency on the primary and structural hydration forces. Additionally, the energy barrier Δ_{pk} (force−distance integral) and magnitude of the primary hydration peak (F_{pk}) adjacent to the interface are recorded in Table 3. Both values were measured from the secondary minimum to the primary maximum (see Figure 1).

From Table 3, the mean hydration layer spacing for the three solutions was $\sigma_{avg} = 3.11 \pm 0.70$ Å, in comparison with a value of 2.5 ± 0.03 Å previously measured with SFA and the expected value from the geometry of the molecule, 2.8 Å.[16] While the values reported here are slightly larger than expected, this is considered to be an artifact of force curve alignment and averaging as illustrated by the smaller hydration layer spacing observed for a single force−distance curve in Figure 1. Nevertheless, it is important to present data from a series of force curves in order to demonstrate statistically significant results. The hydration layer spacing obtained here also agrees with a recent publication of Fukuma et al.[42] under high salt conditions. For comparison, the hydrated radii of Na^+ and Mg^{2+} are 3.6 and 4.3 Å, while the bare ionic radii of Na^+ and Mg^{2+} are 95 and 65 pm respectively.[8] The similarities in the hydration layer spacing measured for both monovalent and divalent species indicate that the structural hydration forces we observe are due to the removal of individual water layers, consistent with the model of Pashley,[12] rather than the removal of hydrated cations, as was recently reported for SFA experiments.[43]

Table 2. Classification of Force Curve Shape for Water, NaCl, and $MgCl_2$ Solutions[a]

	water		150 mM NaCl		150 mM $MgCl_2$	
hydration layers	no.	%	no.	%	no.	%
0	64	30.2	12	5.7	13	5.5
1	**137**	**64.6**	42	19.9	36	15.3
2	8	3.8	**142**	**67.3**	**152**	**64.4**
3	3	1.4	15	7.1	35	14.8
total	212	100	211	100	236	100

[a]Boldface type indicates the most frequent classification for each solution.

The difference in our observations in comparison to SFA measurements is attributed to the geometrically constrained nature of SFA measurements compared to the unconstrained FM-AFM measurements. In SFA, two macroscale mica surfaces are brought together at a constant velocity, forcing out the intervening molecules and thus significantly increasing the local concentration and inhibiting the diffusion of hydrated ionic species (diffusion rates are reduced by at least 2 orders of magnitude).[26] By contrast, our experiments employ an atomically sharp silicon tip that is vertically oscillating at kilohertz frequencies with an amplitude approximating the diameter of a single water molecule. This system results in the measurement of the average tip−surface interaction over the time scale of the measurement and as such implicitly allows for molecules to freely diffuse into and out of the tip−sample gap during the measurement. By use of the Einstein−Smoluchowski diffusion equation, the time required for a water molecule to diffuse 5 Å (the peak−peak amplitude of the tip) is ~0.125 ns.[44] By contrast, the time to complete one oscillation cycle of the tip is ~10 μs, thus allowing for ~80 000 water molecule diffusion time scales to occur per oscillation of the cantilever. Given that the cantilever is approaching the surface at a rate of 1 nm/s and each approach curve contains 2000 data points, each data point represents a change in the mean tip−sample distance of ~0.01 Å with ~100 cantilever oscillations being averaged per data point. Under these conditions, the tip has a maximum instantaneous velocity of ~150 μm/s in contrast to the maximum instantaneous velocity of a water molecule across this small distance (less than two molecular diameters) of ~4 m/s, which is ~32 000 times the maximum tip velocity. Since the water molecules are able to relax to equilibrium, orders of

dx.doi.org/10.1021/ja310255s | J. Am. Chem. Soc. 2013, 135, 2628−2634

Table 3. Fitting Parameters and Calculated Values for Water, NaCl, and $MgCl_2$ Solutions

	A_S, mJ·m^{-2}	λ_S, Å	σ_S, Å	A_P, mJ·m^{-2}	λ_P, Å	Δ_{pk}, kT	F_{pk}, pN
water[a]	2.1 ± 0.14	0.65 ± 0.02	2.18 ± 0.02	9 ± 0.06	4.85 ± 0.04	0.24 ± 0.16	13.3 ± 1.5
150 mM NaCl	10.7 ± 0.08	2.44 ± 0.02	3.47 ± 0.01	10 ± 0.08	2.36 ± 0.02	0.57 ± 0.06	29.1 ± 1.8
150 mM $MgCl_2$	9.5 ± 0.32	2.44 ± 0.06	3.59 ± 0.02	42 ± 0.60	1.53 ± 0.02	1.61 ± 0.02	51.9 ± 0.9

[a]Full fit values: A_S = 9.7 ± 0.41 mJ·m^{-2}, λ_S = 1.85 ± 0.09 Å, and σ_S = 4.43 ± 0.07 Å. Structural hydration parameters are from partial fit (shown in Figure 3).

magnitude faster than the time over which the cantilever is probing them, we consider the data in the paper to have been collected under equilibrium conditions with free diffusion occurring throughout.

Since the use of an atomically sharp AFM tip does not induce lateral confinement (as would be the case for blunt AFM tips and SFA) nor continuous vertical confinement, the increased local concentration (at least an order of magnitude for SFA)[26] and reduced diffusion rate effects are not inherent to this technique. It is precisely the presence or absence of confinement effects to which we attribute the differences in the observed hydration forces for different techniques. Thus, the direct comparison of SFA (two macroscale interfaces approaching) with AFM (a nanoscale object approaching a macroscale interface) and beam scattering experiments[45] (a single macroscale interface) is considered to be nontrivial, as it is likely that the nature of the measurement applied results in a different outcome dependent upon the perturbation of the system. Our AFM technique, which does not induce macroscale confinement, would arguably be the better analogue for a nanoscale object (such as a nanoparticle or biomolecule) approaching an interface, since its influence on the local fluid structure and ion distribution at the interface is minimized[28] and as such represents a more relevant measure of the forces associated with such interactions.

Figure 3 demonstrates that the presence of ions in solution reduces the decay length of the primary hydration force while increasing its magnitude, with divalent cations having a greater effect than monovalent cations for the same concentration. Examining Δ_{pk} and F_{pk} values demonstrates that the presence of ions in solution increases the structural hydration magnitude (inducing stability) of ordered water layers adjacent to a mica surface. Here we observe that the interrelationship between the primary and structural hydration forces appears to be additive, with the magnitude of the structural hydration force independent of ion valency for the same concentration. This is in contrast to the observed nonadditive relationship for concentration effects, indicating a complex interplay between the primary and structural hydration forces, which may be due to differing underlying mechanisms (a topic for further investigation). Again, we see no evidence of secondary hydration forces in our experiments with all decay lengths observed below 5 Å. Our values for A_P and λ_P are consistent with previously reported values for AFM and SFA experiments (A_P = 10^{-3}–10 J·m^{-2} and λ_P = 2–4 Å), where secondary hydration forces were also absent.[9,35]

The comparison of interaction forces for solutions under equivalent electrolytic conditions can be made for the case of 500 mM NaCl (Debye = 4.3 Å) and 150 mM $MgCl_2$ (Debye = 4.5 Å). Here it was observed that A_P increased by ∼80% while λ_P increased by ∼55% for the divalent species when compared to the monovalent cation. Since both decay lengths are significantly below that expected from the electrolytic contributions, this further highlights the inadequacy of continuum models to describe the data. It is interesting to note that both solutions exhibit a similar degree of attraction due to forces such as van der Waals interactions. It is likely that the interplay between primary and structural hydration force is a complex combination of charge effects, hydration affinity, surface affinity, and the size and polarizability of the cations. Previously we have demonstrated that protrusions corresponding to the dimensions of dehydrated cations can be identified at the mica interface in aqueous solutions when the tip–sample distance is small enough (<2.5 Å) to exclude the final layer of interfacial water.[46] These protrusions were found to correlate with the location of negatively charged sites associated with oxygen triads in the basal plane, and their density was shown to scale with cation valency for a fixed concentration. These results, combined with the absence of both structural hydration forces with a spacing corresponding to the hydrated cation size and secondary hydration forces in this study, are in agreement with hydration ion exclusion from the surface hydration layer.[11,34] We propose that at the interface both anions and cations are free to diffuse both laterally and vertically, although the anions are unlikely to be directly interacting with the tip or surface due to their negative charge. The anions in this case are more likely to contribute to the entropic and ion dispersion forces, which occur at longer length scales then those observed in this study. This freely diffusing system then results in a diffuse charge cloud in the vicinity of the tip rather than a system of static charges, since the time scale of the measurement is far longer than that required for diffusion. It is the properties of this diffuse charge layer that we attribute to the nature of the observed primary hydration forces. While we observe no direct evidence of hydrated cations in the tip–sample gap, this is not a direct indication of their absence at the interface, merely that the approach of a nanoscale body is not directly impeded by their presence. This result is not unexpected since the approach of the tip would increase the entropic energy required for a hydrated ion in the gap. Since free diffusion is occurring at time scales much shorter than the AFM force measurement, we expect that the hydrated ions diffuse out of the region beneath the tip during its approach to the interface. Structural hydration forces are, however, detected for water molecules in the same region due to the concentration of water molecules at the interface inducing lateral confinement.[28] It is expected that at very high cation concentrations, where there is an interfacially induced ordering of hydrated cations at the interface, the approach of a nanoscale object may be directly influenced by their presence.

The observed concentration relationship, whereby the primary and structural hydration forces are shown to be nonadditive, is attributed to the complex nature of the interplay between these forces. Whereas the structural hydration force is detected due to modulation of the density of the water molecules directly beneath the tip due to interface-induced ordering, the primary hydration force is detected due to the effects of the diffuse charge cloud at the interface, which is

expected to consist of both an entropic and electrostatic contribution. Complete isolation of such effects is beyond the scope of this study and remains a topic of continued experimental and theoretical interest. Here we simply demonstrate that in the absence of confinement the effects associated with changing the concentration of a monovalent cation at an interface result in nonadditive behavior, while changes in cation valency give rise to an additive relationship between primary and structural hydration forces.

CONCLUSION

Here we present the first direct observations of both primary and structural hydration forces as a function of ion valency and concentration for a nanoscale object approaching an interface. We observe that, in the absence of lateral confinement, the magnitude of the measured hydration forces can be described by a model including only primary and structural hydration contributions, thus allowing for the quantification of their properties and the interrelationship between them. For increasing ion valency and concentration, a trend is observed whereby the magnitude of the primary hydration force is increased while the decay length is decreased. By comparing the relative contributions of the two hydration forces, we are able to observe conditions that maximize the observation of structural hydration adjacent to a charged interface, which has important consequences for obtaining atomic-resolution images in aqueous environments (see Supporting Information). Differences between our observations and previous studies are attributed to the geometry of the system with an atomically sharp tip probing the near contact region. This geometry does not induce ordering due to confinement and does not hinder the diffusion of water/hydrated ions within the tip−sample gap. As the secondary hydration force is attributed to the entropic contribution of the hydrated ions confined between interfaces, it is perhaps not surprising that our unconstrained geometry yields no evidence of secondary hydration. The asymmetric nature of the silica mica interaction in our experiments may also be a source of deviation from previous studies of symmetric systems. The absence of secondary hydration forces, combined with observations of additive behavior for changes in valency contrasted with nonadditive behavior for changes in concentration, leads us to the conclusion that the interactions between nanoscale objects with macroscale interfaces in aqueous environments are substantially more complex than existing models imply (see Parsegian and Zemb[9] and Parsons et al.[7] for a detailed discussion). While we have proposed a diffuse charge cloud mechanism to explain our observations, our experiments raise the question of the feasibility of a ubiquitous model for describing the role of ions in determining solvation forces. With multiple length scales, geometric considerations, and multiple time scales within a single experiment, a substantial body of experimental data would be a key requirement in determining the feasibility of such a ubiquitous model. The need to further develop our understanding of the role of ions and their effects on hydration forces is highlighted by the continuing interest in understanding the interaction of nanoscale objects at interfaces in processes such as nanoparticle deposition and protein adsorption.

ASSOCIATED CONTENT

Supporting Information

One figure showing atomic resolution imaging in the presence of structural hydration forces and additional text explaining how the imaging mechanism is related to the force distance relationship. This material is available free of charge via the Internet at http://pubs.acs.org.

AUTHOR INFORMATION

Corresponding Author

jason.kilpatrick@ucd.ie

Present Address

[†]Faculty of Engineering and Green Technology, Department of Electronic Engineering, Universiti Tunku Abdul Rahman, Perak, Malaysia.

Author Contributions

[‡]These authors contributed equally to this work.

Notes

The authors declare no competing financial interest.

ACKNOWLEDGMENTS

This work was supported by Science Foundation Ireland (Grant 07/IN1/B931).

REFERENCES

(1) Pashley, R. M. *J. Colloid Interface Sci.* **1981**, *80*, 153−162.
(2) Chapel, J. P. *Langmuir* **1994**, *10*, 4237−4243.
(3) Lis, L. J.; McAlister, M.; Fuller, N.; Rand, R. P.; Parsegian, V. A. *Biophys. J.* **1982**, *37*, 657−65.
(4) Kralchevsky, P. A.; Danov, K. D.; Basheva, E. S. *Curr. Opin. Colloid Interface Sci.* **2011**, *16*, 517−524.
(5) Rau, D. C.; Lee, B.; Parsegian, V. A. *Proc. Natl. Acad. Sci. U.S.A.* **1984**, *81*, 2621−2625.
(6) Valle-Delgado, J. J.; Molina-Bolívar, J. A.; Galisteo-González, F.; Gálvez-Ruiz, M. J. *Curr. Opin. Colloid Interface Sci.* **2011**, *16*, 572−578.
(7) Parsons, D. F.; Boström, M.; Lo Nostro, P.; Ninham, B. W. *Phys. Chem. Chem. Phys.* **2011**, *13*, 12352−67.
(8) Jacob, N. *Intermolecular and Surface Forces*, 2nd ed.; Academic Press: London, 1992.
(9) Parsegian, V. A.; Zemb, T. *Curr. Opin. Colloid Interface Sci.* **2011**, *16*, 618−624.
(10) Fukuma, T.; Higgins, M. J.; Jarvis, S. P. *Biophys. J.* **2007**, *92*, 3603−3609.
(11) Parsons, D. F.; Ninham, B. W. *Colloids Surf., A* **2011**, *383*, 2−9.
(12) Pashley, R. M. *Adv. Colloid Interface Sci.* **1982**, *16*, 57−62.
(13) Pashley, R. M. *J. Colloid Interface Sci.* **1981**, *83*, 531−546.
(14) Pashley, R. M.; Israelachvili, J. N. *J. Colloid Interface Sci.* **1984**, *97*, 446−455.
(15) Pashley, R. M.; Israelachvili, J. N. *J. Colloid Interface Sci.* **1984**, *101*, 511−523.
(16) Israelachvili, J. N.; Pashley, R. M. *Nature* **1983**, *306*, 249−250.
(17) Ebeling, D.; Van den Ende, D.; Mugele, F. *Nanotechnology* **2011**, *22*, No. 305706.
(18) Jarvis, S. P.; Uchihashi, T.; Ishida, T.; Tokumoto, H.; Nakayama, Y. *J. Phys. Chem. B* **2000**, *104*, 6091−6094.
(19) Fukuma, T. *Sci. Technol. Adv. Mater.* **2010**, *11*, No. 033003.
(20) Sheikh, K. H.; Jarvis, S. P. *J. Am. Chem. Soc.* **2011**, *133*, 18296−18303.
(21) Butt, H.-J. *Biophys. J.* **1991**, *60*, 1438−1444.
(22) Paunov, V. N.; Binks, B. P. *Langmuir* **1999**, *15*, 2015−2021.
(23) Spitzert, J. J. *Langmuir* **1992**, *8*, 1659−1662.
(24) Marčelja, S. *Colloids Surf., A* **1997**, *129−130*, 321−326.
(25) Besseling, N. A. M. *Langmuir* **1997**, *13*, 2113−2122.
(26) Leng, Y. *Langmuir* **2012**, *28*, 5339−5349.
(27) Trokhymchuk, A.; Henderson, D.; Wasan, D. *J. Colloid Interface Sci.* **1999**, *210*, 320−331.
(28) Kaggwa, G. B.; Nalam, P. C.; Kilpatrick, J. I.; Spencer, N. D.; Jarvis, S. P. *Langmuir* **2012**, *28*, 6589−6594.
(29) Fukuma, T.; Jarvis, S. P. *Rev. Sci. Instrum.* **2006**, *77*, No. 043701.

(30) Kilpatrick, J. I.; Gannepalli, A.; Cleveland, J. P.; Jarvis, S. P. *Rev. Sci. Instrum.* **2009**, *80*, No. 023701.
(31) Sader, J. E.; Jarvis, S. P. *Appl. Phys. Lett.* **2004**, *84*, 1801.
(32) Hutter, J. L.; Bechhoefer, J. *Rev. Sci. Instrum.* **1993**, *64*, 1868−1873.
(33) Pashley, R. M. *J. Colloid Interface Sci.* **1981**, *83*, 531−546.
(34) Ninham, B. W.; Duignan, T. T.; Parsons, D. F. *Curr. Opin. Colloid Interface Sci.* **2011**, *16*, 612−617.
(35) Butt, H.-J.; Cappella, B.; Kappl, M. *Surf. Sci. Rep.* **2005**, *59*, 1−152.
(36) Raviv, U.; Klein, J. *Science* **2002**, *297*, 1540−3.
(37) Yotsumoto, H.; Yoon, R.-H. *J. Colloid Interface Sci.* **1993**, *157*, 434−441.
(38) Adler, J. J.; Rabinovich, Y. I.; Moudgil, B. M. *J. Colloid Interface Sci.* **2001**, *237*, 249−258.
(39) Hogg, R.; Healy, T. W.; Fuerstenau, D. W. *Trans. Faraday Soc.* **1966**, *62*, 1638−1651.
(40) Parsegian, V. A.; Gingell, D. *Biophys. J.* **1972**, *12*, 1192−1204.
(41) Horn, R. G.; Smith, D.; Haller, W. *Chem. Phys. Lett.* **1989**, *162*, 404−408.
(42) Fukuma, T.; Onishi, K.; Kobayashi, N.; Matsuki, A; Asakawa, H. *Nanotechnology* **2012**, *23*, No. 135706.
(43) Espinosa-Marzal, R. M.; Drobek, T.; Balmer, T.; Heuberger, M. P. *Phys. Chem. Chem. Phys.* **2012**, *14*, 6085−6093.
(44) Islam, M. A. *Phys. Scr.* **2004**, *70*, 120−125.
(45) Fenter, P.; Sturchio, N. C. *Prog. Surf. Sci.* **2004**, *77*, 171−258.
(46) Loh, S.-H.; Jarvis, S. P. *Langmuir* **2010**, *26*, 9176−9178.